

Superluminescent diode using narrow-stripe selective area growth at 1.3- μm wavelength

SHUAI ZHOU^{a,*}, JING ZHANG^a, SHANG-JUN LIU^a, KUN TIAN^a, FU-BIN PANG^b

^aChongqing Optoelectronics Research Institute, Chongqing 400060, China

^bElectric Power Research Institute of State Grid Jiangsu Electric Power Co., Ltd., Nanjing 211103, China

The performance and reliability of 1.3- μm InGaAsP/InP superluminescent diode with a narrow-stripe selective area growth structure are reported. The one-step forming active material and passive optical waveguide of active region are grown in a metal organic chemical vapor deposition system. A 4.4-mW fundamental-transverse-mode output power is obtained under injected current 200mA and 25°C, and the full-width at half maximum of the spectrum is 45.7nm. From the result of accelerated aging test carried out for 3744 hours at the ambient temperature of 85°C, the extrapolated life is more than 7.3 years at an ambient temperature of 25°C.

(Received October 22, 2020; accepted August 16, 2021)

Keywords: Superluminescent diode, Narrow-stripe selective area growth, Accelerated aging test, Lifetime

1. Introduction

Superluminescent diodes (SLDs) are attracting widely attention and investigation due to their broad emission spectrum and high power, which are required in many applications, such as fiber optic gyro (FOG)[1-3], optical coherence tomography (OCT)[4, 5], wavelength-division multiplexing (WDM) system testing[6], etc. High performance SLDs fabricated with cost effective and reliable process are in high demand. In the conventional fabrication process of buried heterostructure SLD, active mesa stripe is formed by semiconductor etching followed by a regrowth process. An alternative is selective area growth (SAG). This SAG method could be used to form active material and passive optical waveguide directly, which can result in flat (111)B and (100) plane growth and low propagation loss. It no longer requires semiconductor etching for waveguide formation, which will cause non-uniformity, roughness, and low reproducibility of the waveguide. SAG structure can avoid oxidation problems in the traditional etching process of InGaAlAs waveguide, which maybe cause reliability problems. As a result of material composition and thickness changes, SAG on a semiconductor substrate covered with a patterned SiO₂ mask can also control the bandgap energy of active layer

by changing the SiO₂ mask width during epitaxial growth.

A high-quality growth condition could be obtained by optimizing mask stripe width and direction, growth temperature and pressure, V/III ratio, etc[7-11]. Many types of semiconductor devices, such as InP/InGaAs heterojunction bipolar transistor (HBT)[12], photovoltaic device[13], 1.5- μm InGaAsP/InP superluminescent diode[14], 1200nm ~ 1700nm tunnel junction ultra-broadband semiconductor optical amplifier (SOA)[15], multi-wavelength DFB laser array[16], extended range tunable laser source[17], have been demonstrated using SAG method. It is noteworthy that only very few works about SLD with SAG structure have been reported.

In this work, we intend to fabricate bulk material InGaAsP/InP SLDs with the narrow-stripe SAG structure. In order to obtain fundamental-transverse-mode output SLD, the window width has to be narrow enough, such as 3 μm or less. Firstly, in section 2, theoretical aspect, which is important for the successful design of new SLD structure, is discussed on the basis of modeling approach. The fabrication process of SLD is also described. In section 3, experimental results are described and discussed. To verify the reliability of the SLD devices, long-term accelerated aging tests were also carried out in

this section. Finally, in section 4, the results of this paper are summarized and conclusions are given.

2. Simulation and experimental section

In this section, a numerical simulation of the SLD is carried out by the rate equation and traveling-wave equation[18]. The length, thickness and width of $\text{In}_{1-x}\text{Ga}_x\text{As}_y\text{P}_{1-y}$ direct bandgap lattice-matching ($x=0.47y$, $y=0.63$) bulk-material rectangle active region are $400\mu\text{m}$, $0.2\mu\text{m}$, and $2.8\mu\text{m}$, respectively. Fig. 1(a) shows the simulation results of output power spectra for different bias currents. As shown in the figure, the output powers exhibit Gaussian-shaped spectra. As the current increases, the peaks of the spectra shift from $\sim 1330\text{nm}$ to $\sim 1290\text{nm}$, which can be attributed to the band-filling effect. The spectrum ripple increases with increasing current, and Ghazal et. al.[19] have demonstrated that an almost linear relation between ripple and output power. Fig. 1(b) shows the total light output power as a function of current.

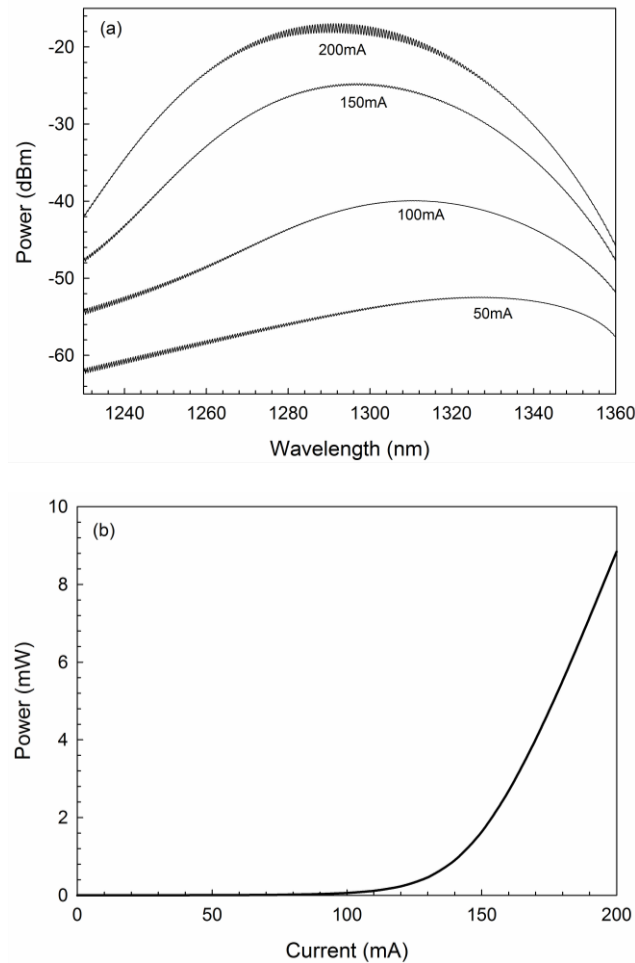


Fig. 1. Simulation results of output power spectra (a) and total light output power (b) for different bias currents

Samples were grown in a metal organic chemical vapor deposition (MOCVD) system. Fig. 2 shows a schematic view of the narrow-stripe selective MOCVD InGaAsP/InP bulk material SLD fabrication process. (a) Pairs of $0.1\text{-}\mu\text{m}$ -thick SiO_2 mask stripe were patterned by plasma enhanced chemical vapor deposition (PECVD) on a (100) oriented Sn-doped InP substrate to form $3.0\text{-}\mu\text{m}$ -wide window stripe w_1 in between. The mask stripes were formed along the [011] direction and the mask width w_2 was $5\mu\text{m}$ in our experiment. (b) Selective active layer growth was performed at a pressure of 100mbar, a temperature of 630°C , and a V/III ratio of 80. Source materials were trimethylindium (TMIn), triethylgallium (TEGa), arsine (AsH_3), and phosphine (PH_3). Epitaxial layers form bottom to top were $0.3\text{-}\mu\text{m}$ -thick n-InP buffer layer, $0.08\text{-}\mu\text{m}$ -thick 1.1Q InGaAsP undoped lower waveguide layer, $0.2\text{-}\mu\text{m}$ -thick 1.3Q InGaAsP active layer, $0.08\text{-}\mu\text{m}$ -thick 1.1Q InGaAsP undoped upper waveguide layer, and $0.07\text{-}\mu\text{m}$ -thick p-InP upper cladding layer. The growth rates were $22\text{nm}/\text{min}$, $20\text{nm}/\text{min}$, and $10\text{nm}/\text{min}$ for InP, 1.1Q InGaAsP, and 1.3Q InGaAsP, respectively. Then, the selectively grown layers were surrounded by smooth (100) and (111)B crystal planes. (c) The p-n current blocking layers were grown by unselective regrowth method after removing the SiO_2 mask stripes using $1\text{HF}:5\text{NH}_3\text{F}:1\text{H}_2\text{O}$. The current blocking layers form bottom to top were $0.4\text{-}\mu\text{m}$ -thick p-InP, $0.02\text{-}\mu\text{m}$ -thick 1.1Q p-InGaAsP etching stop layer, and $0.4\text{-}\mu\text{m}$ -thick n-InP. (d) After depositing $0.1\text{-}\mu\text{m}$ -thick SiO_2 mask by PECVD, a current channel was then dug by both dry etching and wet etching, and the n-type current blocking layer just over the narrow stripe active layer was removed. (e) Then, the p-InP cladding layer and p-InGaAs contact layer were grown. (f) Finally, the current channels and electrodes were fabricated. In order to suppress lasing oscillation which results from the simulated emission and multiple reflections at facets, we introduced a $600\text{-}\mu\text{m}$ -long (L_2) absorbing region with a $400\text{-}\mu\text{m}$ -long pumped region (L_1) structure, as is shown in Fig. 4(a). The structure reduces light feedback into the active layer, and the estimation value of reflectivity was calculated to be 1.57×10^{-4} , following the procedure outlined by Utaka[20].

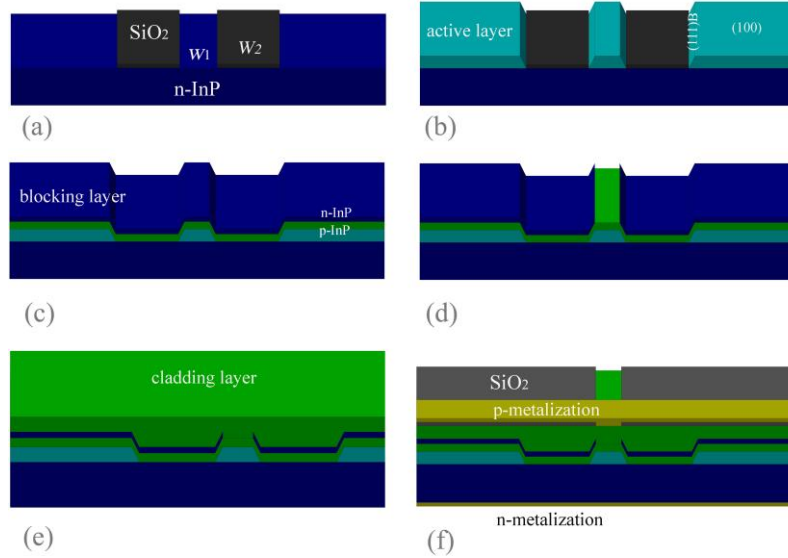


Fig. 2. Schematic of device fabrication process (color online)

After alloying, the wafer was cleaved into bars and the facets were deposited with a 168nm-thick single layer zirconia antireflection (AR) coating in electron beam evaporator equipment. As is shown in Fig. 3, the possible range of reflectivity was calculated by the optical admittance method[21], when considering a fabrication deviation ($\pm 5\text{nm}$) of thickness. A reflectivity, superior to 0.6×10^{-2} , was obtained. Fig. 4(b) shows the cross-sectional scanning electron microscope (SEM) image of the light-emitting area before coating. A Trapezoid InGaAsP active region with a basic angle of 55° was formed and the bottom width was about $2.8\mu\text{m}$. Then, the SLD bars were cleaved into chips and soldered to AlN heat-sink with p-side face upward. In our investigation of the power and spectral characteristics, we mounted SLD sample on a Peltier thermoelectric element. Current was injected from a stabilized direct current (DC) source and the spectra were measured by coupling into a single-mode fiber.

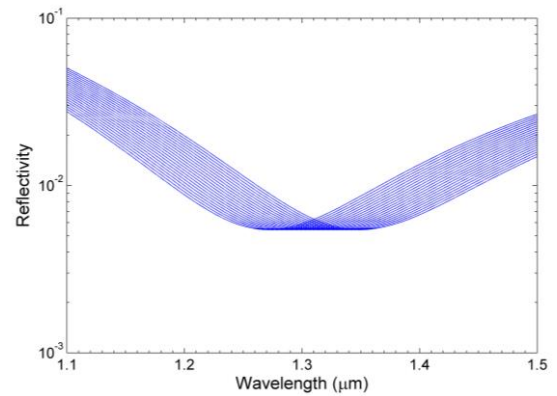


Fig. 3. The calculated reflectivity range when considering a fabrication deviation (color online)

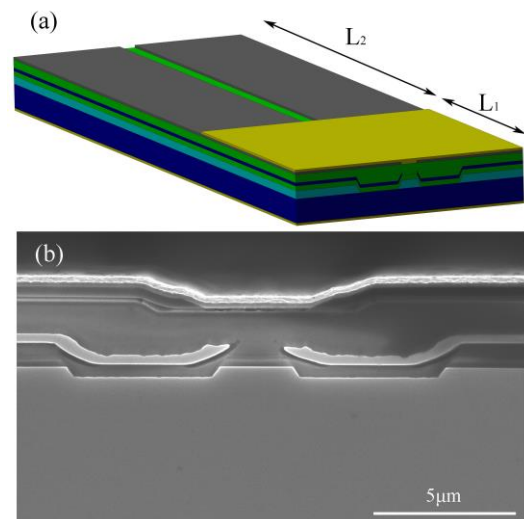


Fig. 4. Schematic device structure (a) and cross-sectional SEM image (b) (color online)

3. Result and discussion

The optical spectra and powers from the front facet side were measured. The spectra measured at direct-current levels of 50mA, 100mA, 150mA, and 200mA are shown in Fig. 5. They were measured using a YOKOGAWA AQ6370 optical spectrum analyzer with 0.02nm resolution. The peak wavelengths are 1314.1nm, 1306.8nm, 1312.3nm, and 1316.4nm, respectively. At low injected current, the peak wavelength drops because the band-filling effect (corresponding to spontaneous emission). Then it gradually increases as the current increases (corresponding to amplified spontaneous emission), because it mainly depends on the bandgap narrowing effect due to a temperature rise of the active region[22] and the increasing injected carrier density[18], and the carrier band-filling effect can be neglected since the carrier concentration is nearly clamped in the amplified spontaneous emission mode. The wavelength shift coefficient is about 95.9nm/A in the linear region from 50mA to 200mA in our experiment, which is also seriously affected by the heating-sinking capability of the submount. The full-width at half maximum (FWHM) of the spectrum changes from 41.3nm to 45.7nm and the corresponding coherence length, $L_{\text{coh}} \approx \lambda^2/\text{FWHM}$ [23], lies between 36.9 μm and 40.8 μm for SLD with different injections. Fig. 6 shows the light output power versus direct-current (P - I) curve. The maximum output power of SLD with the SAG method was 4.4mW at a submount temperature of 25 $^{\circ}\text{C}$.

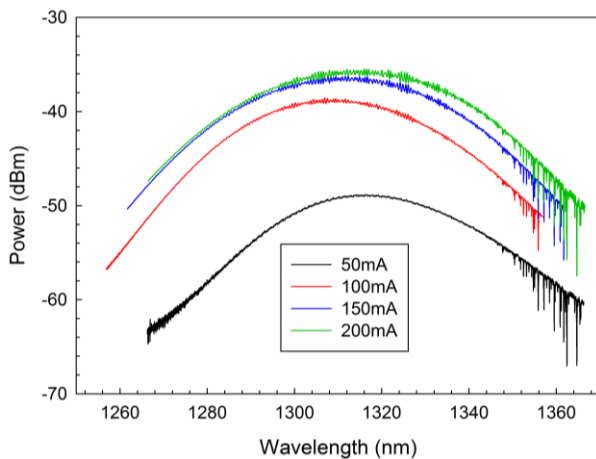


Fig. 5. Spectra of the SLD measured at different current levels (color online)

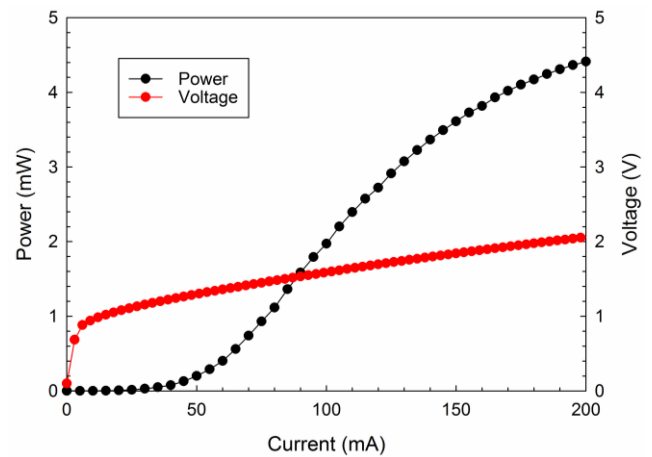


Fig. 6. P - I - V characteristics of the SLD device at a submount temperature of 25 $^{\circ}\text{C}$ (color online)

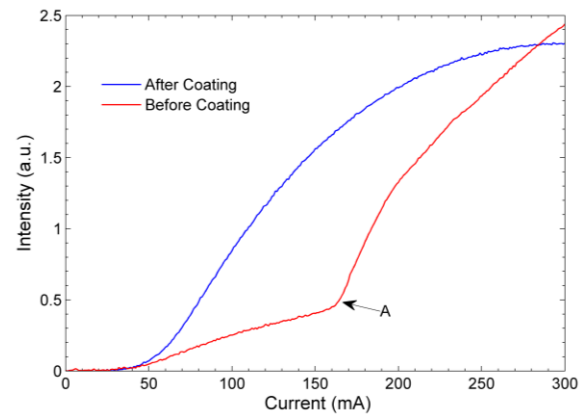


Fig. 7. P - I characteristics of the SLD device before and after coating (color online)

The output power against pulse-current (P - I) characteristics before and after depositing AR coating on the chip are shown in Fig. 7. It is found that there is no clear threshold point below 160mA (point A) before coating, which is due to the optical feedback suppression by absorbing region. Then, above 160mA, the light intensity of stimulated emission increases, and the light intensity of the spontaneous emission increases because of the AR coating. Following the procedure[24, 25], we have calculated the loss coefficient α of the devices. Fig. 8 shows the measured output power characteristic versus the active region length with driving current density J as a parameter. Current density J_0 at the threshold current could be determined by the illustration. When $J = J_0$, the output power is linearly proportional to active region length L_1 , and J_0 is about 1.8KA/cm 2 . At $J > J_0$, the output power is an exponential function of active region length. Then, we calculated the loss coefficient

$\alpha=32.0/\text{cm}$, using the power ratio $P(l_1)/P(l_2)$ of two active region lengths l_1 and l_2 at the current density $5\text{KA}/\text{cm}^2$.

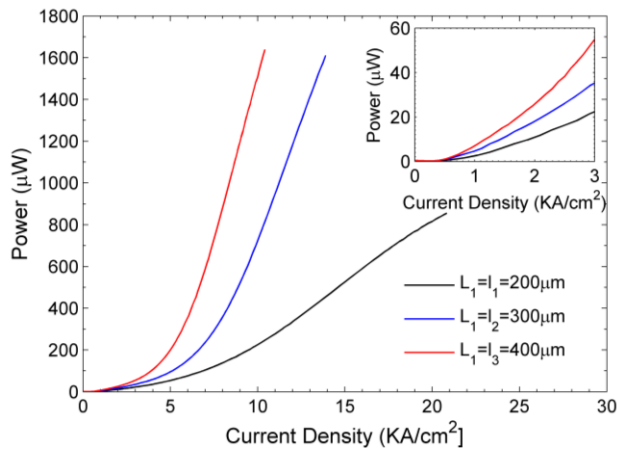


Fig. 8. Output power characteristics as a function of the active length (color online)

To investigate the reliability of the SLD, accelerated aging test was carried out using 100mA under 85°C , and the output powers of SLDs were re-measured under 100mA at room temperature to establish the amount of degradation induced by high temperature operation. As shown in Fig. 9, five SLD-COS samples were aged at constant current for 3744h. By considering a drift of -20% of output power as the failure criteria, the average lifetime was calculated using linear extrapolation and estimated to be 6553h at 85°C . We use the minimum activation energy allowed by the Telcordia recommendation GR-468-CORE, i.e. 0.35eV. Then, the SLDs' mean time to failure (MTTF) at 25°C could be obtained by calculating Arrhenius relation[26], $\text{MTTF}=7.3$ years.

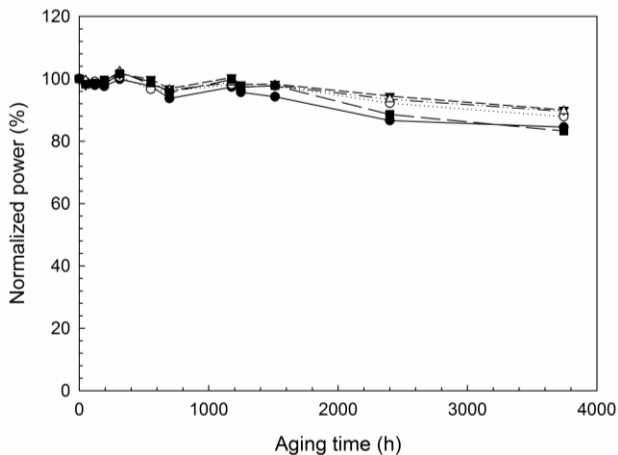


Fig. 9. Accelerated aging output power data of SLD samples

4. Conclusion

In this paper, devoted to the 1.3- μm InGaAsP/InP SLD with a narrow-stripe SAG structure, we have reported performance and reliability. We modeled the output spectra and light output power for different bias currents by solving the rate equation and traveling-wave equation. We fabricated the device samples and described the optical characteristics such as the optical power and the emission spectra. The characteristics of SLD were obtained at 25°C by using a Peltier thermoelectric element. We achieved the output power of 4.4mW at a driving current of 200mA. The accelerated aging test was carried out for 3744h at ambient temperature of 85°C . The results indicated that life exceeding 7.3 years at 25°C .

Acknowledgements

This work was supported by State Grid Electric Power Co., Ltd. (Grant No. 5700-202018483A-0-0-00).

References

- [1] Q. Wang, C. Yang, X. Wang, Z. Wang, *Opt. Lett.* **38**(24), 5422 (2013).
- [2] S. Zhou, J. Zhang, L. Duan, Z. Tang, G. Deng, *Mod. Phys. Lett. B* **30**(5), 1650046 (2016).
- [3] A. Kafar, S. Stanczyk, M. Sarzynski, S. Grzanka, J. Goss, I. Makarowa, A. Siwinska, T. Suski, P. Perlin, *Photonics Res.* **5**(2), A30 (2017).
- [4] D. S. Adler, T. H. Ko, A. K. Konorev, D. S. Mamedov, V. V. Prokhorov, J. J. Fujimoto, S. D. Yakubovich, *Quantum Electron.* **34**(10), 915 (2004).
- [5] N. Ozaki, S. Yamauchi, Y. Hayashi, E. Watanabe, H. Ohsato, N. Ikeda, Y. Sugimoto, K. Furuki, Y. Oikawa, K. Miyaji, D. Childs, R. Hogg, *J. Phys. D: Appl. Phys.* **52**, 225105 (2019).
- [6] D. D. Sampson, W. T. Holloway, *Electron. Lett.* **30**(19), 1611 (1994).
- [7] W. Feng, J. Q. Pan, F. Zhou, H. Yang, L. Zhao, H. Zhu, W. Wang, *Semicond. Sci. Technol.* **21**, 841 (2006).

- [8] Y. Sakata, K. Komatsu, *J. Electron. Mater.* **29**(1), 37 (2000).
- [9] D. Kapolnek, S. Keller, R. Vetry, R. Underwood, P. Kozodoy, S. Baars, U. Mishra, *Appl. Phys. Lett.* **71**(9), 1204 (1997).
- [10] Y. Sakata, Y. Inomoto, K. Komatsu, *J. Cryst. Growth* **208**, 130 (2000).
- [11] K. Kudo, T. Sasaki, M. Yamaguchi, *J. Cryst. Growth* **170**, 634 (1997).
- [12] Y. Dong, Y. L. Okuno, U. K. Mishra, *J. Cryst. Growth* **260**, 316 (2004).
- [13] H. Goto, K. Nosaki, K. Tomioka, S. Hara, K. Hiruma, J. Motohisa, T. Fukui, *Appl. Phys. Express* **2**, 035004 (2009).
- [14] J. H. Song, K. Kim, Y. A. Leem, G. Kim, *IEEE Photonics Technol. Lett.* **19**(19), 1415 (2007).
- [15] F. Choa, in EOS 2006-19th Annual Meeting of the IEEE Lasers and Electro-Optics Society, IEEE (2006).
- [16] F. Soares, M. F. Baier, Z. Zhang, T. Gaertner, D. Franke, J. Decobert, M. Achouche, D. Schmidt, M. Moehrle, N. Grote, M. Schell, in 2016 Compound Semiconductor Week (CSW) [Includes 28th International Conference on Indium Phosphide & Related Materials (IPRM) & 43rd International Symposium on Compound Semiconductors (ISCS)], IEEE (2016).
- [17] F. Lemaitre, S. Latkowski, C. Fortin, N. Lagay, R. Pajkovic, E. Smalbrugge, J. Decobert, H. Ambrosius, K. Williams, in 2018 IEEE Photonics Conference (IPC), IEEE (2018).
- [18] M. J. Connelly, *IEEE J. Quantum Electron.* **37**(3), 439 (2001).
- [19] O. M. S. Ghazal, D. T. Childs, B. J. Stevens, N. Babazadeh, R. A. Hogg, K. M. Groom, *Semicond. Sci. Technol.* **31**(4), 045003 (2016).
- [20] K. Utaka, S. Akiba, K. Sakai, Y. Matsushima, *IEEE J. Quantum Electron.* **QE-20**(3), 236 (1984).
- [21] J. Lee, T. Tanaka, S. Sasaki, S. Uchiyama, M. Tsuchiya, T. Kamiya, *J. Lightwave Technol.* **16**(5), 884 (1998).
- [22] S. Zhou, Z. Tang, S. Liu, Y. Zhou, J. Zhang, L. Duan, K. Tian, K. Zhao, C. Feng, *Phys. status solidi A* **215**, 1800176 (2018).
- [23] A. Semenov, V. Batovrin, I. Garmash, V. Shidlovsky, M. Shramenko, S. Yakubovich, *Electron. Lett.* **31**(4), 314 (1995).
- [24] Y. Kashima, A. Matoba, H. Takano, *J. Lightwave Technol.* **10**(11), 1644 (1992).
- [25] T. Lee, C. A. Burrus, B. I. Miller, *IEEE J. Quantum Electron.* **QE-9**(8), 820 (1973).
- [26] K. Luo, A. K. Chin, Z. Xu, A. Nelson, W. Gao, in High-Power Fiber and Semiconductor Lasers, Proceeding of SPIE, **4993** (2003).

*Corresponding author: zscetc44@gmail.com